# A novel cell culture system modeling the SARS-CoV-2 life cycle

Xiaohui Ju[1], Yunkai Zhu[2], Yuyan Wang[2], Jingrui Li[3], Jiaxing Zhang[4], Mingli Gong[1], Wenlin Ren[1], Sai Li[4,5], Jin Zhong[6], Qiangfeng Cliff Zhang[4,5], Rong Zhang[2], Qiang Ding[1,5*]

[1] School of Medicine, Tsinghua University, Beijing 100084, China

[2] Key Laboratory of Medical Molecular Virology (MOE/NHC/CAMS), School of Basic Medical Sciences, Shanghai Medical College, Biosafety Level 3 Laboratory, Fudan University, Shanghai 200032, China

[3] State Key Laboratory of Plant Physiology and Biochemistry, College of Biological Sciences, China Agricultural University, Beijing 100193, China

[4] School of Life Sciences, Tsinghua University, Beijing 100084, China

[5] Beijing Advanced Innovation Center for Structural Biology, Tsinghua University, Beijing 100084, China

[6] Unit of Viral Hepatitis, CAS Key Laboratory of Molecular Virology and Immunology, Institut Pasteur of Shanghai, Chinese Academy of Sciences, Shanghai, 200031, China

[*]Correspondence to Qiang Ding, qding@tsinghua.edu.cn

# ABSTRACT

Severe acute respiratory syndrome coronavirus 2 (SARS-CoV-2) causes the global pandemic of COVID-19, and no effective antiviral agents and vaccines are available. SARS-CoV-2 is classified as a biosafety level-3 (BLS-3) agent, impeding the basic research into its biology and the development of effective antivirals. Here, we developed a biosafety level-2 (BSL-2) cell culture system for production of transcription and replication-competent SARS-CoV-2 virus-like-particles (trVLP). This trVLP expresses a reporter gene (GFP) replacing viral nucleocapsid gene (N), which is required for viral genome packaging and virion assembly (SARS-CoV-2-GFP/ΔN trVLP). The complete viral life cycle can be achieved and exclusively confined in the cells ectopically expressing SARS-CoV or SARS-CoV-2 N proteins, but not MERS-CoV N. Genetic recombination of N supplied *in trans* into viral genome was not detected, as evidenced by sequence analysis after one-month serial passages in the N-expressing cells. Moreover, intein-mediated protein trans-splicing approach was utilized to split the viral N gene into two independent vectors, and the ligated viral N protein could function *in trans* to recapitulate entire viral life cycle, further securing the biosafety of this cell culture model. Based on this BSL-2 SARS-CoV-2 cell culture model, we developed a 96-well format high throughput screening for antivirals discovery. We identified salinomycin, tubeimoside I, monensin sodium, lycorine chloride and nigericin sodium as potent antivirals against SARS-CoV-2 infection. Collectively, we developed a convenient and efficient SARS-CoV-2 reverse genetics tool to dissect the virus life cycle under a BSL-2 condition. This powerful tool should accelerate our understanding of SARS-CoV-2 biology and its antiviral development.


**Key words**: SARS-CoV-2, COVID-19, Reverse genetics, intein, drug screening.

# INTRODUCTION

The coronavirus disease 2019 (COVID-19) caused by severe acute respiratory syndrome coronavirus 2 (SARS-CoV-2) is an ongoing pandemic[1]. As of 1 December 2020, more than 63.7 million cases of COVID-19 have been reported, resulting in more than 1.5 million deaths. Severe patients died of breathing difficulty to acute respiratory distress. Up to now, there is still no vaccine and antiviral agents available[2].

SARS-CoV-2 belongs to the genus *Coronavirus*, the family *Coronaviridae*, and the order *Nidovirales*. Its genome is a single-stranded, positive-sense RNA with similar specific gene characteristics of known coronaviruses[3]. The viral genome encodes non-structural proteins, structural proteins and accessory proteins. The non-structural proteins carry all of the enzymatic activities important for viral replication. For example, the genome encodes an RNA-dependent RNA-polymerase complex (nsp7, nsp8 and nsp12), RNA capping machinery (nsp10, nsp13, nsp14 and 16) and additional enzymes such as proteases (the nsp3 PLpro and the nsp5 3CLpro) which cleave viral polyproteins[4,5]. Structural proteins include surface (S), envelope (E), membrane (M), and nucleocapsid (N) proteins[6]. The S, E and M proteins are embedded within the lipid envelope. The primary function of N protein is to package the ~30 kb single stranded, 5′-capped positive-strand viral genome RNA into a ribonucleoprotein (RNP) complex. Ribonucleocapsid packaging is a fundamental part of viral self-assembly, and the RNP complex constitutes the essential template for replication by the RNA-dependent RNA polymerase complex[7]. In addition, the N protein has been shown to modulate the host antiviral responseand may play regulatory roles in the viral life cycle[3]. The accessory proteins, encoded by ORF3a, ORF6, ORF7a, ORF7b, and ORF8 genes, are not directly involved in viral replication but interfere with the host innate immune response or are of unknown function[3,8,9].

The development of reverse genetics systems of coronavirus has profoundly advanced the study of this large-sized RNA virus. The cDNA of the coronavirus RNA genome is constructed using bacterial artificial chromosomes (BACs), in vitro ligation of CoV cDNA fragments, or vaccinia viral vector[10]. Recently, a SARS-CoV-2 full-

length cDNA clone has been established using the *in vitro* ligation of cDNA fragments[11,12]. This system has been shown to be efficient for the recovery of infectious virus, and a reporter gene can be inserted into the viral genome to monitor virus replication, providing a good tool for high-throughput antiviral screening. However, experimentations involving live virus are restricted to BSL-3 laboratories, which hinders the study of SARS-CoV-2 and development of countermeasures. Therefore, it is urgent to develop an efficient non-BSL-3 experimental system for SARS-CoV-2. Herein, we developed an N-based genetic complementation system to produce biologically contained, and transcription, replication-competent SARS-CoV-2 virus-like particles lacking N gene (SARS-CoV-2 ΔN trVLP). The lack of the viral N protein could be genetically complemented *in trans* by ectopic expression in packaging cells to produce the SARS-CoV-2 ΔN trVLP. SARS-CoV-2 ΔN trVLP could be propagated and passaged in the packaging cells while only results in single-round infection in wild-type cells. We applied this cell culture model for SARS-CoV-2 biology, antiviral evaluation and novel antivirals discovery.

# RESULTS

## Design and assembly of SARS-CoV-2-GFP/ΔN genome

Nucleocapsid translated from a subgenomic RNA of SARS-CoV-2 has multiple functions and its primary function is participation in genomic RNA package and virus particle release. To test whether the function of N could be complemented *in trans*, we constructed SARS-CoV-2-GFP/ΔN genome, in which we replaced the regions encoding viral N (from nucleotides position 28274 to 29533) based on MN908947 genome with GFP reporter gene, and Caco-2 cells, an immortalized cell line of human colorectal adenocarcinoma cells, as packaging cell lines which stably express viral N protein by lentiviral transduction (**Fig. 1**).

To assemble the molecular clone of SARS-CoV-2-GFP/ΔN genome, we utilized an *in vitro* ligation approach, which has been used for constructing the infectious clone of SARS-CoV-2[11,12]. We divided the full-length cDNA of SARS-CoV-2-GFP/ΔN genome into a set of five fragments (A, B, C, D and E) and each fragment can be obtained by PCR using the chemically synthesized viral genome (MN908947 strain) as the template. Each DNA fragment was flanked by a type IIS restriction endonuclease site (BsaI or BsmBI) that ensures unidirectional assembly of intermediates into a full-length cDNA. In addition, we engineered a T7 promoter upstream of fragment A and a poly(A) tails at the downstream of fragment E, allowing for *in vitro* transcription of capped, polyadenylated transcript of viral genome (**Fig. 1A**).

The five PCR-amplified DNA fragments were digested with BsaI or BsmBI to generate specific sticky ends (**Fig. 1B**). The digested fragments were further purified and were ligated by T4 DNA ligase at 4°C to generate the full-length cDNA of SARS-CoV-2-GFP/ΔN genome. The resulting 29.4-Kbp *in vitro* ligation products were confirmed by agarose gel electrophoresis (**Fig. 1C**). Next, this *in vitro* ligation products were used as the template for *in vitro* transcription with the T7 RNA polymerase to generate the RNA transcript of SARS-CoV-2-GFP/ΔN genome (**Fig. 1D**).

## Recovery and propagation of SARS-CoV-2-GFP/ΔN trVLP

Caco-2 cells are highly permissive for SARS-CoV-2 infection. As the recombinant

SARS-CoV-2-GFP/ΔN virus like particles, lacking N gene, could potentially propagate in the cells supplied with viral N protein *in trans*, we established the Caco-2 cells stably expressing viral N gene by lentiviral transduction (designated as Caco-2-N cells). The expression of N was confirmed by flow cytometry and immunoblotting assay (**Fig. S1A, B and Fig. 1E**).

Next, we sought to recover SARS-CoV-2-GFP/ΔN trVLP, the *in vitro* transcribed RNA transcript of viral genome was electroporated into Caco-2-N cells. Within 48h, GFP fluorescence can be readily observed, suggesting that viral genome replication and transcription occurs in the cell. After 96h, cytopathic effects (CPEs) were observed in the electroporated Caco-2-N cells, suggesting that the recombinant SARS-CoV-2-GFP/ΔN trVLP was produced and propagated (**Fig. S2**). We collected the cell culture supernatants (denoted as passage 0 (P0) virus), and inoculated them to Caco-2 or Caco-2-N cells (**Fig. 2A**). GFP signal can be readily observed within 48 h, and further expanded within 72 h in Caco-2-N cells, whereas no signal was detected in Caco-2 cells (**Fig. 2B**). Cells were collected for immunoblotting and RT-qPCR analysis at 72 h post-infection to detect viral spike antigen and RNA abundance. Consistent with the GFP expression, we could detect viral spike expression and high abundance of viral RNA in the Caco-2-N cells but not in Caco-2 cells (**Fig. 2C and D**). RT-PCR analysis using a primer set outside the N-encoding region confirmed that the N gene was indeed replaced by GFP in the recombinant trVLP viral genome (**Fig. 2E**).

To characterize the SARS-CoV-2-GFP/ΔN trVLP infection, two spike-specific mAbs (1F11 and 2F6)[13] were tested for their ability to neutralize infection of Caco-2-N cells. A neutralizing mAb specific for HIV gp120 (VRC-01) was also included as the control[14]. The mAbs were incubated with SARS-CoV-2-GFP/ΔN trVLP for 1 h at 37°C, and the trVLP–mAb mixtures were tested for infection of Caco-2-N cells, respectively. Viral infection was determined by flow cytometry at 48 h post-infection, and the results showed that 1F11 and 2F6 inhibited trVLP infection in a dose-dependent manner; in contrast, VRC01 had no effect on the trVLP infection (**Fig. 2F**).

Soluble recombinant forms of the human ACE2 are able to bind SARS-CoV-2

spike protein and inhibit its interaction with cellular ACE2[15,16]. We therefore tested the ability of mouse IgG Fc fusion proteins of soluble human ACE2 (D30E) (hACE2 (D30E)-Fc)[16] to inhibit SARS-CoV-2-GFP/ΔN trVLP infection. F10scFv, an antibody specifically targeting HA of the Influenza A virus, was used as a negative control. The hACE2 (D30E)-Fc trVLP showed a dose-dependent neutralization of infectivity, inhibiting SARS-CoV-2-GFP/ΔN infection of Caco-2-N cells by 70% at 0.5μg/ml (**Fig 2G**). Together, these data demonstrated that the infection of SARS-CoV-2-GFP/ΔN trVLP recapitulates that of wild-type virus as its virus entry is also mediated by the interaction between viral spike and host ACE2.

**Characterization of the genetic stability of SARS-CoV-2-GFP/ΔN trVLP**

Next, we sought to characterize the genetic stability of SARS-CoV-2-GFP/ΔN trVLP. For this purpose, we analyzed the rescued SARS-CoV-2-GFP/ΔN trVLP in Caco-2-N cells after 10 passage. The cell culture supernatants collected from SARS-CoV-2-GFP/ΔN RNA electroporated Caco-2-N cells were defined as P0, and the cell cultures collected from each subsequent passage on the Caco-2-N cells were defined as P1 to P10, respectively. The total RNAs extracted from each cell passage were used to perform RT-PCRs with the pair of primers to amplify the fragment between ORF8 and 3'UTR that covers the region of the inserted GFP reporter gene. (**Fig.3A**). RT–PCR products of 1.5-Kbp and 1-Kbp were expected for WT genome and SARS-CoV-2-GFP/ΔN genome, respectively. SARS-CoV-2-GFP/ΔN trVLP was considerably stable for at least 3 serial passages since the 1-Kb RT–PCR products were detected at P3 trVLP (**Fig. 3B**). The loss of GFP reporter gene was detected in the P4 trVLP as indicated by amplicon of < 1 Kb size (**Fig. 3B, Fig S3A**). No PCR product of greater than 1 Kb was detected in the all samples, suggesting that no heterologous RNA inserted into the SARS-CoV-2-GFP/ΔN genome, at least in the GFP report region.

To characterize the trVLP sequence variations in an unbiased manner, we performed deep sequencing analysis on the P1 and P10 trVLP genome. The deep sequencing analysis provides deep coverage, on the order of 30 million reads per sequencing sample (**Fig. S3B**). Sequences of P1 or P10 were mapped to the SARS-

CoV-2 and SARS-CoV-2-GFP/ΔN trVLP genomes, respectively (**Fig. 3C and D**) and relative abundances of these sequences between P1 and P10, were also compared (**Fig 3E, Fig S3C**). The deep sequencing analysis could not detect N sequences in the both P0 and P10 genome (**Fig. 3C**), and GFP sequences were readily detected in the P1 genome with high abundance, however, it was rarely detected in the P10 genome (**Fig. 3D**), due to GFP sequences deletion (**Fig. 3B, Fig S3A**). Additionally, we found that the subgenomic RNAs of ORF6, ORF7 and ORF8 were dramatically decreased in the P10-trVLP infected cells compared with that of P1 VLP (**Fig. 3E**), indicating that ORF6, ORF7 and ORF8 may not be required for virus infection at least *in vitro*, consistent with other reports that deletions of these regions were observed in clinical samples by deep sequencing analysis[17-20].

**Reconstitution of functional N protein by split intein-mediated protein ligation**

Inteins are intervening protein sequences within a host protein that mediate their self-excision from the precursor protein and ligates the flanking N- and C-terminal fragments (exteins)[21]. Split inteins are a subset of inteins that are expressed as two separate polypeptides at the ends of two host proteins and catalyze their trans-splicing, resulting in the generation of a single larger polypeptide (**Fig. 4A**). To further minimize the chance of recombination of N into the SARS-CoV-2-GFP/ΔN genome, we aimed to split the N gene into two separate elements using a naturally split intein embedded within the catalytic subunit of DNA polymerase III (DnaE) in many species of cyanobacteria (Npu intein)[22]. Npu intein activity is context-dependent, and Cys as first residue in the C-extein is required for efficient trans-splicing. However, there is no Cys residue in SARS-CoV-2 N protein. In order to split the N, we had to find the appropriate splice sites that would have two well-folded, yet stable protein fragments, and also substitute first residue in the C-extein with Cys without disruption of N protein function. To locate the splice sites according to these requirements we chose three splice sites in the N protein, to have the N-intein A152C, S176C and G212C (**Fig. 4A**). As for each of N-intein above, we constructed two lentivirus vectors encoding either the N- or the C-terminal half of the N protein fused to the N- and C-terminal halves of the Npu intein,

having $N^N$-$Int^N$ and $Int^C$-$N^C$, respectively (**Fig. 4A**). Each lentivirus vector included appropriate regulatory elements (promoter and a polyadenylation signal) and a Flag tag to allow detection of the full-length reconstituted N protein (**Fig. 4A**). We then transduced $N^N$-$Int^N$ and $Int^C$-$N^C$ either individually or together in Caco-2 cells, and the full-length N protein reconstitution was assessed by Western blotting assay. We could not detect splicing above negligible levels of N protein by N-intein (A152C) (**lane 2, Fig. 4B**), while N-intein (S176C) and N-intein (G212C) could reconstitute into full-length N protein with S176C or G212C point mutation, respectively (**lane 5 and 8, Fig. 4B**). Next, recombinant SARS-CoV-2 GFP/ΔN trVLP (P1) was inoculated to Caco-2 cells transduced with N-intein as indicated, and GFP fluorescence was detected after two days only in the cells transduced either with a single lentivirus that encodes full-length N or with the combination of N-intein (G212C), but not in the cells with the single N- and C-terminal N-intein (G212C). As expected, GFP fluorescence was also not detected in cells transduced with N-intein (A152C), of which the splicing did not occur; interestingly, N-intein (S176C) could ligate a full-length N (S176C), but fails to support virus infection, suggesting that the S176C mutation probably impairs N protein function (**Fig. 4C and D**). Consistent with the GFP expression, the subgenomic RNA of E can be readily detected in cells transduced either with a single lentivirus that encodes full-length N or with the combination of N-intein (G212C), but not others (**Fig. 4E**). Together, we showed that the N-intein (G212C) was capable of efficiently trans-splicing to generate a functional N (G212C) protein to support SARS-CoV-2 GFP/ΔN trVLP infection. As the N-intein was split into separate constructs, it would further reduce the potential biosafety concerns of this SARS-CoV-2 GFP/ΔN trVLP cell culture model.

**Residue-specific phosphorylation of N protein is critical for viral infectivity**

Coronavirus N protein is an extensively phosphorylated, highly basic, vital structural protein the primary function of which is to form a helical ribonucleoprotein complex with viral RNA (RNP) as core structure of the virion. A variety of other functions have been ascribed, such as viral genome transcription and replication, or

evasion of antiviral immunity. SARS-CoV-2 N protein is highly homologous to the N protein of SARS-CoV, with 91% identity, while exhibited 48% identity with that of MERS-CoV (**Fig. 5A**). Several proteomics profiling analyses have been performed and reveals that N protein of SARS-CoV-2 is extensively phosphorylated at multiple sites (**Fig. 5A and Fig. S4**). However, the roles of N protein phosphorylation remain unclear. Our N-based genetic trans-complemented cell culture model offers an opportunity to specifically study N protein function in viral life cycle. Firstly, we determined whether SARS-CoV-2 GFP/ΔN trVLP infection can be complemented by N proteins from different coronavirues. We used SARS-CoV-2 GFP/ΔN trVLP to infect the Caco-2 cells transduced with N from SARS-CoV-2, SARS-CoV or MERS-CoV. Two days later, the cell culture supernatants from each cells were collected to infect naive Caco-2 cells transduced with SARS-CoV-2 (Caco-2-N cells as previously used) to test whether SARS-CoV-2 GFP/ΔN trVLP were assembled in the Caco-2 cells transduced with distinct N proteins. Two days later, the Caco-2-N cells were collected and GFP or viral RNA was quantified by flow cytometry or RT-qPCR, respectively (**Fig. 5B and C**). SARS-CoV N protein with 91% identity with that of SARS-CoV-2, but not MERS-CoV N protein with 48% identity with that of SARS-CoV-2, could rescue SARS-CoV-2 GFP/ΔN trVLP, (**Fig. 5D and E**), suggesting that coronavirus N protein has virus-specific mechanism to recognize viral genome to achieve its function, meanwhile, N proteins from SARS-CoV and SARS-CoV-2, with high genetic similarity, have redundant function to some degree.

As SARS-CoV-2 N is heavily phosphorylated at multiple sites especially within the central Ser-Arg (SR)-rich motif, we are interested in the roles of phosphorylation in N function. For this purpose, we mutated S176, S413, S176/413, S105, S183, S188, S206, S188/206 as the conservation of these residues with that of SARS-CoV into alanine to specifically dissect their function. Notably, GSK-3 is the kinase responsible for the phosphorylation of this SR-rich motif in SARS-CoV N protein, which are primed by the phosphorylation of Ser-189 and Ser-207 (Ser-188 and Ser-206 in SARS-CoV-2 N protein accordingly)[23,24]. We generated the Caco-2 cells lentivirally

transduced with the N variants as indicated. As shown in Western blotting assay, the mutations did not alter the protein expression and stability in the Caco-2 cell (**Fig. 5F**), We noted that N with the S188A/S206A double mutations migrated slightly faster than WT and other mutants, probably because blockade of the initial priming phosphorylation would prohibit subsequent phosphorylation events by GSK-3, which was observed in SARS-CoV[23]. Next, we inoculated the Caco-2 cells expressing different N variants with SARS-CoV-2 GFP/ΔN trVLP, and cell culture supernatant was collected 48 h later to infect the naïve Caco-2-N cells, and cells were collected to observe or determine GFP expressing by microscopy or flow cytometry 2 days later. Interestingly, most of the phosphorylation null mutants were able to assemble virus-like particles with comparable or slightly reduced efficiencies than WT. However, S188A/S206A double mutations completely abolish N function (**Fig. 5G-H**), highlighting the critical role of S188 and S206 for N function.

To further investigate whether GSK-3 contributing N protein phosphorylation to regulate virus life cycle, we treated Caco-2-N cells with LiCl or SB216763, which are specific inhibitors of GSK-3 and inoculated cells with SARS-CoV-2 trVLP spontaneously. Two days later, cell culture medium was collected and infect Caco-2-N cells for additional 2 days, and then cells were harvested for flow cytometry analysis of GFP expression. As expected, the LiCl or SB216763 could inhibit GFP expression in a dose-dependent manner, indicating that inhibition of GSK-3 could block N phosphorylation, thus impairing SARS-CoV-2 trVLP production. Given the vital role of the N protein in multiple stages of the viral life cycle, inhibition of N functions by modulating host cell kinases may be viable strategies for combating SARS-CoV-2 infections.

**Evaluation of the antivirals using SARS-CoV-2-GFP/ΔN VLP cell culture model**

To test the utility of this system in anti-viral drug screening, we evaluated the efficacy of IFN-β, remdesivir, GC376, lopinavir, and ritonavir in inhibiting SARS-CoV-2 GFP/ΔN trVLP infection. Caco-2-N-intein (G212C) cells were treated with IFN-β with 0.2–20 pg/ml for eight hours prior to infection. Then cells were infected with

SARS-CoV-2 GFP/ΔN trVLP at a multiplicity of infection (MOI) of 0.05. After 48 h, the cells were collected and GFP fluorescence, the proxy of virus infection, was quantified by flow cytometry analysis. Remarkably, even at 0.2 pg/ml IFN-β we observed 60% reduction of the GFP fluorescence (**Fig. 6A**). This is consistent with recent reports that SARS-CoV-2 is sensitive to type I interferon treatment[11,25-27]. Remdesivir and GC376, which targets virus RNA dependent RNA polymerase (RdRp) and 3CLpro respectively, have been reported to be potent antivirals against SARS-CoV-2[28-32]. Lopinavir and ritonavir-HIV protease inhibitor, is a combination antiviral medicine used to treat HIV[33], which could inhibit SARS-CoV and MERS-CoV infection *in vitro*, and they may target SARS-CoV-2 Nsp5 (3CLpro) to inhibit virus infection. To test potential dose-dependent antiviral activity of those drugs in our system, we incubated Caco-2-N-intein (G212C) cells with various concentrations of those drugs and simultaneously infected the cells with SARS-CoV-2 GFP/ΔN trVLP at a MOI of 0.05. After 2 days, GFP fluorescence was determined (**Fig.6 B-E**). Remdesivir and GC376 exhibited potent antiviral effect with $IC_{50}$=62.5 nM and 4.5 μM respectively, with essentially no apparent cytotoxic effect (**Fig.6 B and C**). In contrast, Lopinavir or ritonavir inhibited SARS-CoV-2 GFP/ΔN trVLP with $IC_{50}$=8.7 uM, or 7.7 uM, while those drugs both show serious cytotoxicity at the $IC_{50}$ concentration (**Fig.6 D and E**), compromising their clinical utilities, which is in line with the fact that lopinavir and ritonavir as no significant beneficial effect was observed in a randomized trial established in March 2020 with a total of 1,596 patients[34].

These results demonstrated that our experimental system can be used for evaluation of antivirals and could be potentially developed for high-throughput screening of antiviral compounds.

**Identification of potent antivirals against SARS-CoV-2 virus using trVLP cell culture model by high-throughput screening**

To provide proof-of-concept that our system could be utilized in high-throughput screening, we performed HTS of Topscience natural product library containing 377 drugs (**Fig. 7A**) and the potential hit compounds were further assessed using authentic

SARS-CoV-2 to confirm the antiviral activities *in vitro*. DMSO or remdesivir were included as the negative or positive control.

Among the 377 compounds of the compound library, 10 hit molecules showed equal or higher inhibition with an inhibitory efficiency ≥ 60% (**Fig. 7A**). In addition, we excluded five hits due to the visible cytotoxicity. This criterion allowed the selection of five hits as the highest confident hits: salinomycin, tubeimoside I, monensin sodium, lycorine chloride and nigericin sodium (**Fig. 7A**). Among these five compounds, lycorine chloride, salinomycin and monensin sodium inhibit HCoV-OC43 infection as previously reported[35] and monensin sodium blocks avian infectious bronchitis virus (IBV) infection[36]. Notably, a recent study demonstrated that salinomycin possessed a potent antiviral activity to inhibit SARS-CoV-2 infection *in vitro*[37], which further demonstrated that our system could be used for HTP antiviral screening. We next determined the $IC_{50}$ of the hit compounds using authentic SARS-CoV-2 virus. Salinomycin showed SARS-CoV-2 antiviral activity with an $IC_{50}$ and $CC_{50}$ of 2.836 and 20.23 μM, respectively, and selectivity index ($SI = CC_{50}/IC_{50}$) of 7.13. In comparison, other four compounds did not show dramatic cytotoxic effect in the tested concentrations. Of note, tubeimosde I exhibited an $IC_{50}$ of 1.371 μM; monensin sodium exhibited an $IC_{50}$ of 0.632 μM; lycorine chloride showed antiviral activity with an $IC_{50}$ of 0.773 μM, and nigericin sodium, exhibited an $IC_{50}$ of 11.25 μM. These results demonstrated that the compounds we identified using SARS-CoV-2 GFP/ΔN trVLP system exhibited potent antiviral activity against authentic SARS-CoV-2 infection, and our screening provided new candidate compounds to effectively treat infection of SARS-CoV-2.

# DISCUSSION

As its high pathogenicity and the lack of effective vaccines and therapeutics, SARS-CoV-2 is classified as a biological safety level 3 (BSL-3) pathogen[38], which has hindered the drug discovery and biological research due to biocontainment requirements. In this study, we developed an *in vitro* cell culture system to produce the recombinant SARS-CoV-2 virus lacking the N-encoding region in the viral genome (SARS-CoV-2 ΔN). Recombinant SARS-CoV-2 ΔN can expand and propagate in packaging cells (Caco-2-N) but results in only single-cycle infection in naïve Vero or Caco-2 cells, which biologically contained the virus in the cells expressing N protein. This BSL-2 SARS-CoV-2 possesses a reporter gene GFP, providing a surrogate readout for authentic viral infection. We monitored the recombinant virus infection in the Caco-2-N cells for one month and NGS sequencing result suggested that no recombination was detected. In addition, we utilized the split intein-mediated protein ligation to reconstitute N function which further ensure the biosafety of this system.

This cell model represents a unique system in the basic research application for better understanding SARS-CoV-2 life cycle. Virus has evolved since its outbreak in the end of last year, and some mutations or deletions have been observed. However, the functional consequences of these mutations or deletions on virus infectivity or pathogenesis is poorly characterized. Herein, we utilized our model system to study the roles of N in the SARS-CoV-2 life cycle. Since N can be expressed alone *in trans*, it is convenient to perform mutagenesis on N to dissect its detailed function. Moreover, the introduction of mutations *in trans*-expressed N will avoid the cis effects of the mutations, for example, the disruption of critical RNA secondary or tertiary structures in the SARS-CoV-2 genome, thereby providing a more appropriate system to specifically evaluate the biological roles of domains, motifs, or amino acid residues within the N protein. Additionally, we inserted a Flag tag at the C terminus of N, which did not impair the ability of N to rescue viral production. With this Flag tag, N can be detected and immunoprecipitated by an anti-FLAG antibody (**Fig. S4A**). Multiple amino acids in N protein can be phosphorylated, but our data demonstrated that most

379 of these phosphorylation may not be required for N function at least *in vitro*. Meanwhile,
380 we also identified numerous host factors associated with N protein (**Fig. S4A; Table**
381 **S2**), notably, we also found that N protein could interact with G3BP1 and G3BP2, the
382 stress granule assembly proteins, which was in line with previous studies[39,40]. Recent
383 studies found that N protein could impair the stress granule assembly to escape the
384 antiviral effect[40,41]. Thus, the trVLP system provides a new tool to study host factors
385 and viral proteins that may interact with N during SARS-CoV-2 infection.

386 Development of effective therapeutics for COVID-19 remains an urgently unmet
387 medical need. This recombinant trVLP recapitulates the complete SARS-CoV-2 life-
388 cycle in the Caco-2-N or Caco-2-N$^{intein}$ cells. The reporter readout of the virus, such as
389 fluorescent proteins or luminescent proteins, offers a rapid, real-time, quantitative and
390 less labor-intensive measures than traditional methods of viral titer reduction.
391 Importantly, the reporter virus-based assay could cooperate with a BSL-2 compatible
392 high-content screening platform to facilitate antiviral screening. Thus, we developed a
393 96-well format to screen the antiviral compounds in the Topscience Natural Compounds
394 Library, and we identified five compounds which could efficiently block SARS-CoV-2
395 infection. Among them, lycorine, salinomycin and monensin have been reported as the
396 potent inhibitors against HCoV-OC43 infection[35], and salinomycin could block SARS-
397 CoV-2 infection as reported recently[37]. Those data further validate the suitability of our
398 trVLP system in drug discovery. In our screening, we identified Tubeimoside I and
399 nigericin sodium as novel compounds which exhibited potent antiviral activities against
400 authentic SARS-CoV-2 infection *in vitro*. Future studies could be performed to evaluate
401 their antiviral activities *in vivo*.

402 Additionally, there is an urgently need for effective vaccines to contain SARS-
403 CoV-2 pandemic[38]. The recombinant SARS-CoV-2 lacking of N gene should provide a
404 new means of vaccine development. The greatest advantage of SARS-CoV-2 ΔN is that
405 this virus possesses all the structural viral proteins to induce humoral immune responses
406 and that, upon infection, it could produce all the nonstructural viral proteins in host cells
407 to induce cell-mediated immune responses. Of course, further studies, especially in

408 animals, are needed to determine the immunogenicity, safety, and efficacy of it.

409 In summary, the biologically contained SARS-CoV-2 trVLP lacking the N gene
410 represents a safe, alternative experimental system to study SARS-CoV-2 biology and
411 to screen antiviral compounds and this novel system will greatly accelerate current
412 SARS-CoV-2 research efforts.
413

## ACKNOWLEGEMENTS

We thank Di Qu, Xia Cai, Zhiping Sun, Wendong Han, and other colleagues at the Biosafety Level 3 Laboratory of Fudan University for help with experiment design and technical assistance. We thank Dr. Guocai Zhong (Shenzhen Bay Laboratory, Shenzhen, China) for generously providing the recombinant ACE2-Fc protein. We thank Prof. Haiteng Deng and Xianbin Meng in Proteinomics Facility at Technology Center for Protein Sciences, Tsinghua University, for protein MS analysis. We thank Dr. Jenna M. Gaska for suggestions and revision of the manuscript. We are grateful to other members of the Ding lab for critical discussions and comments on the manuscript.

This work was supported by Tsinghua-Peking University Center of Life Sciences (045-61020100120), Tsinghua University Initiative Scientific Research Program (2019Z06QCX10), National Natural Science Foundation of China (32041005), National Key Research and Development Program of China (2020YFA0707701), Beijing Advanced Innovation Center for Structure Biology (100300001), Start-up Foundation of Tsinghua University (53332101319), Project of Novel Coronavirus Research of Fudan University (to Y.X.), and Development Programs for COVID-19 of Shanghai Science and Technology Commission (20431900401).

## Potential Competing Interest statements

Q.D. and X.J. have filed a patent application on the use of the SARS-CoV-2 transcomplementation system and its use for anti-SARS-CoV-2 drug screening.

## MATERIALS And METHODS

**Cell culture.** HEK293T, Vero, Vero E6, A549 and Caco-2 cells were maintained in Dulbecco's modified Eagle medium (DMEM) (Gibco, China) supplemented with 10% (vol/vol) fetal bovine serum (FBS), and 50 IU/ml penicillin/streptomycin in a humidified 5% (vol/vol) $CO_2$ incubator at 37°C. All cell lines were tested negative for mycoplasma.

**Cloning of the SARS-CoV-2-GFP/ΔN cDNA.** cDNAs (Wuhan-Hu-1, MN908947) of SARS-CoV-2-GFP/ΔN were synthesized from the GenScript company. PCR was conducted to amplify fragments A, B, C, D and E using high fidelity PrimeSTAR Max DNA Polymerase (Takara). T7 promoter was introduced upstream of 5' UTR of SARS-CoV-2 genome in fragment A. To guarantee a seamless assembly of the full-length cDNA, type IIS restriction endonuclease sites (BsaI or BsmBI) were introduced at both ends of PCR fragments. The primers used for the PCR assay were listed in Supplemental Table 1.

**Assembly of a Full-Length SARS-CoV-2-GFP/ΔN cDNA.** PCR fragments were digested with BsaI or BsmBI restriction enzyme (NEB) to specific sticky end. Digested fragments are purified by E.Z.N.A gel extraction kit (Omega). Fragment A, B are ligated first by T4 DNA ligase (NEB) in 40μl system. At the same time, fragments C, D, E are also ligated in another tube at 4°C for 24 hours. Then, fragment A, B and C, D, E are combined together added with 2μl T4 DNA ligase buffer and 2μl T4 DNA ligase to 100μl at 4°C for another 24 hours. At the end of ligation, we took 5μl product to run an agarose gel to check the efficiency of ligation. Full-length assembly cDNA was phenol/chloroform extracted, isopropanol precipitated, and resuspended in 10μL nuclease-free water.

**RNA *in vitro* transcription, electroporation and virus production.** RNA transcript was *in vitro* transcribed by the mMESSAGE mMACHINE T7 Transcription Kit (ThermoFisher Scientific) in 30μl system with some modifications. Twenty micrograms of viral RNA and 20μg N mRNA were mixed and added to a 4-mm cuvette

466 containing 0.4 mL of Caco-2-N cells ($8\times10^6$) in Opti-MEM. Single electrical pulse was
467 given with a GenePulser apparatus (Bio-Rad) with setting of 270V at 950μF. GFP signal
468 can be observed 17 hours post electroporation. Three days post electroporation, P0 virus
469 was collected and Caco-2-N cells were infected with P0 virus to amplify virus.
470 **Lentivirus packaging.** Vesicular stomatitis virus G protein (VSV-G) pseudotyped
471 lentiviruses were produced by transient cotransfection of the third-generation
472 packaging plasmids pMD2G (catalog no. 12259; Addgene), psPAX2 (catalog number
473 12260; Addgene) and the transfer vector pLVX by VigoFect DNA transfection reagent
474 (Vigorous) into HEK293T cells. The medium was changed 12 h post transfection.
475 Supernatants were collected at 36, 60 and 84 h after transfection, pooled, passed
476 through a 0.45-μm filter, aliquoted, and frozen at -80°C refrigerator.
477 **RNA isolation and RT-qPCR.** Total cellular RNA was isolated using TRNzol reagent
478 (Thermo, 15596018). To analyze the RNA level of SARS-CoV-2 in infected cells,
479 quantitative real-time PCR was performed. In brief, 1μg total RNA was reverse
480 transcribed using ReverTra Ace qPCR RT Kit (TOYOBO, FSQ-101) to produce cDNA
481 with random primers. Reactions of qPCR were carried out using the 2×RealStar Green
482 Power Mixture (Genstar, A311) according to the instruction. The qPCR primers for
483 viral RNA were as follows: THU-2190 (5'- CGAAAGGTAAGATGGAGAGCC-3')
484 and THU-2191 (5'- TGTTGACGTGCCTCTGATAAG-3'). The sequences of the qPCR
485 primers for GAPDH was described previously[42]. Relative expression levels of the target
486 genes were calculated using the comparative cycle threshold (CT) method. All data
487 were normalized relative to the housekeeping gene GAPDH.
488 **RNA-seq and data analysis.** Total RNA was extracted by using TRIzol™ Reagent
489 (Invitrogen) according to the manufacturer's protocol. The rRNAs were removed by
490 using Ribo-Zero Gold module of Illumina TruSeq stranded total RNA library prep kit
491 (RS-122-2201) and then cDNA libraries were constructed according to the
492 manufacturer's protocol. RNA-seq was performed by using the Illumina Novaseq
493 platform. The reference genome of SARS2 (MN908947) was downloaded from
494 https://www.ncbi.nlm.nih.gov/nuccore /MN908947. After removing low-quality

reads, remaining Illumina sequence reads were mapped to human (GRCh38) and SARS2 genome by using HISAT2.1.0 with parameters: --rna-strandness RF –dta. RNA-seq coverage was visualized by using Integrative Genomics Viewer (IGV). To quantifiy the expression levels of SARS2 genes, RPKM of each virus genes and GFP gene were calculated. Heatmaps were drawn by using R package "pheatmap" (https://www.r-project.org). To quantify the junction-reads from subgenomic RNAs, the STAR2.7.5c was used for reads mapping. The junction-reads was defined and collected as described in Kim, Cell, 2020. A Sankey diagram was drawn by using R packages named "networkD3" and "dplyr".

**IFN-β, neutralizing antibody and drug treatment.** To assess the antiviral efficacies of the materials, $1\times10^4$ Caco-2-N cells were seeded into 96-well plates. After 12h, cells were infected with SARS-CoV-2-GFPΔN virus at MOI of 0.05. For neutralizing antibody treatment, virus was incubated with neutralizing antibody for 1 hour at 37°C before infection. For IFN-β (Sino Bioligical, 10704-HNAS-5) test, cells were pre-treated with IFN-β for 8 hours before infection. For remdesivir (MedChemExpress, HY-104077), lopinavir (biochempartner, BCP01395) or ritonavir (biochempartner, BCP03777) treatment, drugs were added simultaneously upon infection. Two days after infection, flow cytometry was performed to analyze GFP positive rate. The 50% inhibitory concentrations (IC50; compound concentration required to inhibit viral replication by 50% reduction of GFP positive cells) were determined using logarithmic interpolation using GraphPad Prism software version 7.0.

**Cell viability assay.** Caco-2-N cells were seeded into 96-well plate ($1\times10^3$ cells/well). After 12 hours, cells were treated with drugs with different concentrations. Cell viability was measured two days post treatment with CellTiter-Glo Luminescent Cell Viability Assay kit (Promega, G7570) following standard protocol. In brief, cells in 100 μl culture medium were added with 100 μl CellTiter-Glo reagent. After 15 minutes, luminescence was recorded with GloMax (Promega). $CC_{50}$ was determined using logarithmic interpolation using GraphPad Prism software version 7.0.

**Flow cytometry analysis.** Cells were detached in PBS containing 0.02% EDTA and

524 then washed once with cold PBS. Cells were then fixed in 4% PFA for 30 minutes at
525 room temperature. Fixed cells were resuspended in PBS and analyzed by LSRFortessa
526 SORP (BD Biosciences) and FlowJo software.
527 **Western blotting.** Sodium dodecyl sulfate-polyacrylamide gel electrophoresis (SDS-
528 PAGE) immunoblotting was conducted as follows: After trypsinization and cell
529 pelleting at 1500 r/m for 10 min, whole-cell lysates were harvested in cell lysis buffer
530 (50 mM Tris-HCl [pH 7.5], 150mM NaCl, 1% NP-40, 1mM EDTA) supplemented with
531 protease inhibitor cocktail (Sigma). Lysates were electrophoresed in 4-12%
532 polyacrylamide gels and transferred onto PVDF membrane. The blots were blocked at
533 room temperature for 0.5 h using 5% nonfat milk in 1× phosphate-buffered saline (PBS)
534 containing 0.1% (v/v) Tween 20. The blots were exposed to primary antibodies anti-N
535 (05-0154, AbMax), S (40589-T62, Sino Biological), β-Tubulin (CW0098, CWBIO),
536 Flag (F7425, Sigma), ACE2 (10108-T24, Sino Biological) in 5% nonfat milk in 1×PBS
537 containing 0.1% Tween 20 for 2 h. The blots were then washed in 1×PBS containing
538 0.1% Tween 20. After 1h exposure to HRP-conjugated secondary antibodies and
539 subsequent washes were performed as described for the primary antibodies.
540 Membranes were visualized using the Luminescent image analyzer (GE).
541 **Antiviral screening.** Twelve hours prior to infection for the antiviral screening $5 \times 10^4$
542 Caco-2-$N^{int}$ cells were seeded in 96 well plates. The next day, a single dilution of each
543 compound of the Topscience Natural Product Library at 5 μM final concentration was
544 added to the cells (50 μL/well). DMSO or remdesivir (3.5μM) were included in each
545 plate as the internal control. After 2 hours, 50 μL of virus was added to the wells at MOI
546 0.05. Two days after infection, cells were collected for flow cytometry analysis to
547 determine the GFP expression.
548 **Evaluation of antiviral activity using authentic SARS-CoV-2 virus.** A549 cells
549 stably expressing human ACE2 were seeded in a 96-well plate ($4\times10^4$ cells/well). Next
550 day, cells were treated with drugs (Lycorine chloride (TargetMol, T2774), Tubeimoside
551 I (TargetMol, T2715), Nigericin sodium (TargetMol, T3092), Monensin sodium
552 (MedChemExpress, HY-N0150), Salinomycin (MedChemExpress, HY-15597)) of

different concentration for 2 hours prior to infection. Cells were infected with SARS-CoV-2 at an MOI of 1 for 1 h, washed three times with PBS, and incubated in 2% FBS culture medium for 24 h for viral antigen staining. Cells were fixed with 4% paraformaldehyde in PBS, permeablized with 0.2% Triton X-100, and incubated with the rabbit polyclonal antibody against SARS-CoV nucleocapsid protein (Rockland, 200-401-A50, 1μg/ml) at 4 °C overnight. After three washes, cells were incubated with the secondary goat anti-rabbit antibody conjugated with Alexa Fluor 555 (Thermo #A32732, 2 μg/ml) for 2 h at room temperature, followed by staining with 4',6-diamidino-2-phenylindole (DAPI). Images were collected using an Operetta High Content Imaging System (PerkinElmer). For high content imaging, two biological replicates for each concentration of drug were scanned and five representative fields were selected for each well of 96-well plates. Image analysis was performed using the PerkinElmer Harmony high-content analysis software 4.9. Cells were automatically identified by DAPI (nuclei). Mean fluorescent intensity of channel Alexa 555 (viral nucleocapsid) of each cell were subsequently calculated, respectively. For the 0% inhibition control, cells were infected in the presence of vehicle only. The $IC_{50}$ value was defined as the concentration at which there was a 50% decrease in N protein expression. Data were analyzed using GraphPad Prism 7.0. The $IC_{50}$ values were calculated by nonlinear regression analysis using the dose-response (variable slope) equation (four parameter logistic equation).

**Statistical analysis.** Student's *t* test or one-way analysis of variance (ANOVA) with Tukey's honestly significant difference (HSD) test was used to test for statistical significance of the differences between the different group parameters. *P* values of less than 0.05 were considered statistically significant.

**Data availability.** RNA-seq dataset generated here can be found in the aforementioned NCBI Gene Expression Omnibus (GEO Accession no. GSE162629, https://www.ncbi.nlm.nih.gov/geo/query/acc.cgi?acc=GSE162629). Other data from this study are available upon request from the corresponding author.

583 **FIGURES AND FIGURE LEGENDS**

584

Figure 1

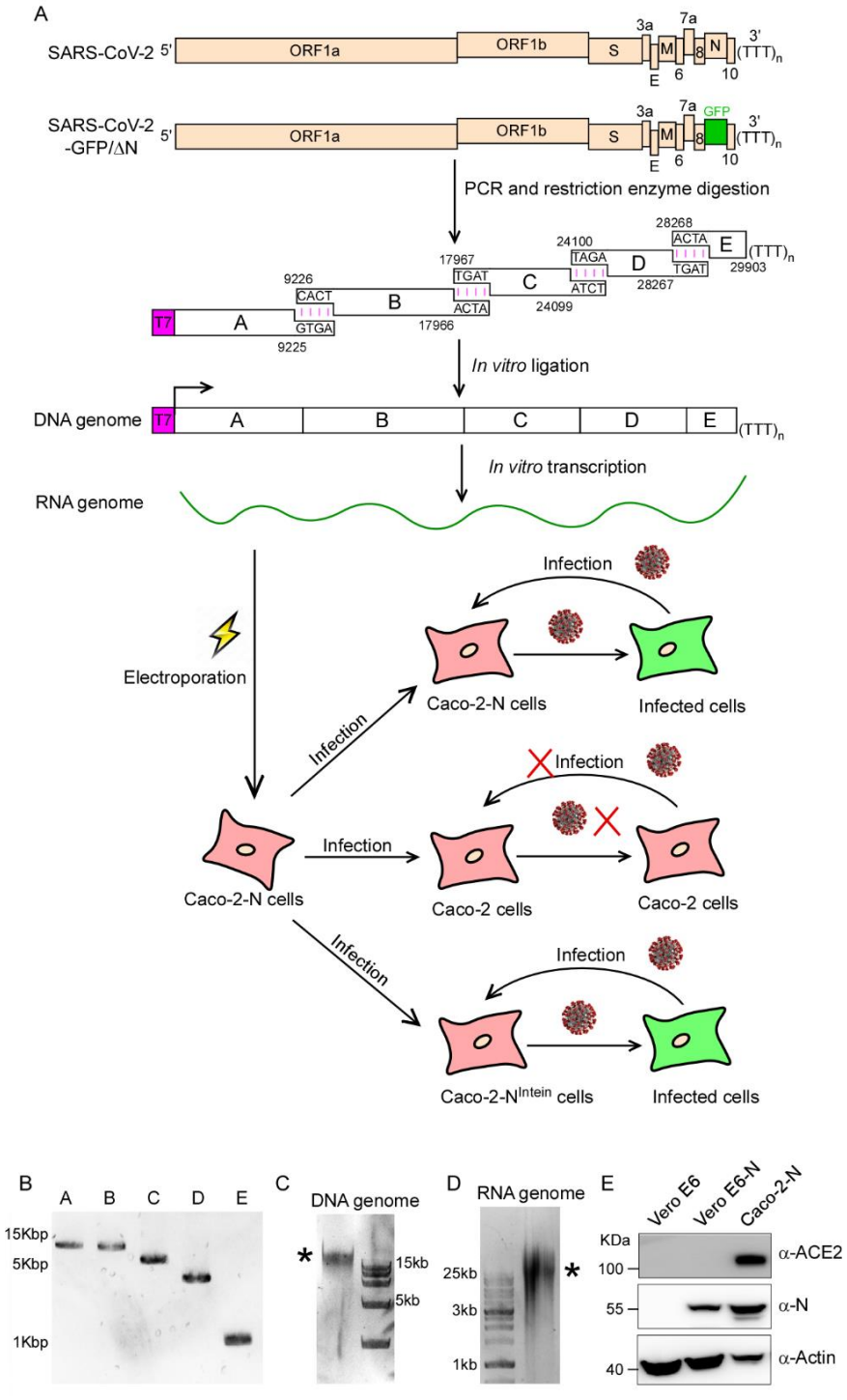

585 **Figure 1. Production of SARS-CoV-2 GFP/ΔN trVLP.** (A) The top rows show
586 genetic organizations of the SARS-CoV-2 and SARS-CoV-2 GFP/ΔN genomes. The
587 ORF of N is replaced with reporter gene (GFP here). The cDNA of SARS-CoV-2
588 GFP/ΔN genome was divided into five fragments designated as Fragment A, B, C, D
589 and E, which could be obtained by PCR (B). Each cDNA fragment was flanked by a
590 class IIS restriction endonuclease site (BsaI or BsmBI) and the nucleotide sequences
591 and locations of the cohesive overhangs are indicated. The fragment cDNA were
592 digested and purified for directed assembly of SARS-CoV-2 GFP/ΔN cDNA (see *C*
593 panel, and the star indicates the genome-length cDNA), which served as the template
594 for *in vitro* transcription to generate viral RNA genome (see D panel, and the star
595 indicates the genome-length RNA transcript). The viral genomic RNAs were
596 electroporated into Caco-2-N cells. After 3 days, the supernatant was collected and
597 inoculated with Caco-2 or Caco-2-N cells. (E). Western blotting assay was performed
598 to detect the expression of N proteins and ACE2 in Caco-2-N cells, Vero E6 and Vero
599 E6-N cells.
600
601

602

Figure 2

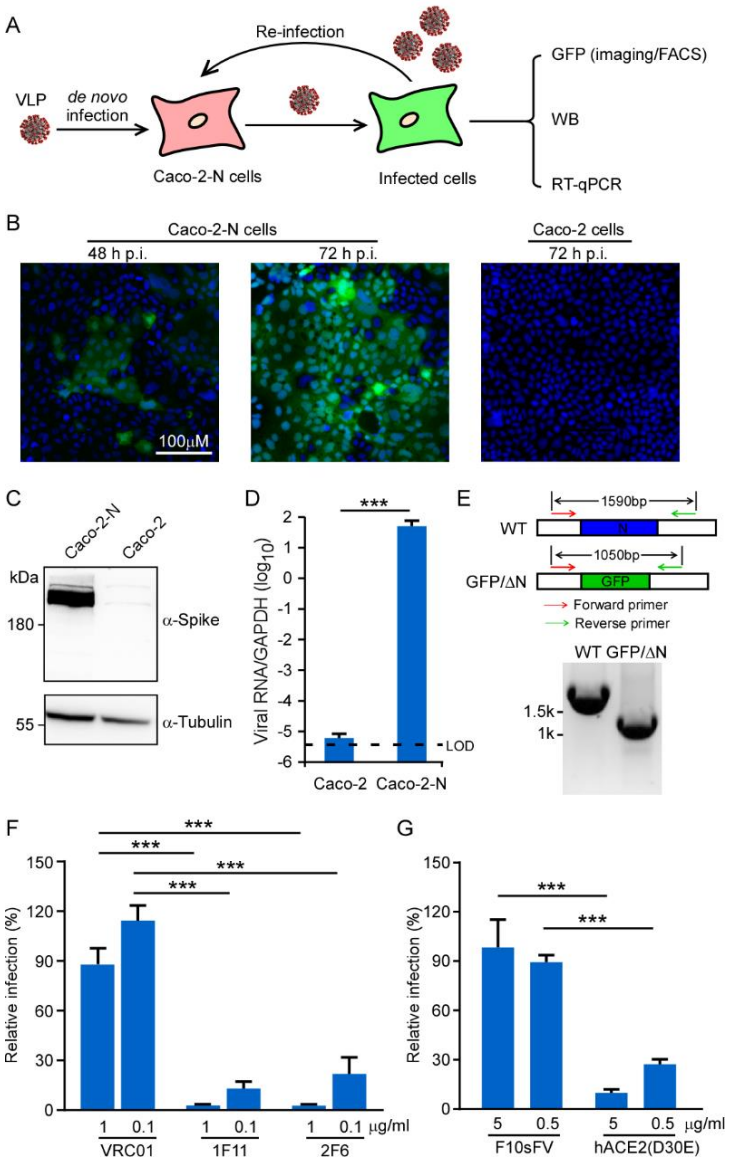


603

604 **Figure 2. The recombinant SARS-CoV-2 GFP/ΔN trVLP can propagate with the**
605 **help of viral N protein.** (A) Experimental scheme. Caco-2 or Caco-2-N cells were
606 infected with SARS-CoV-2 GFP/ΔN for 3h (MOI 0.05), washed, and incubated for an
607 additional 72 h. GFP fluorescence were observed or quantified by microscopy or flow
608 cytometry analysis. Viral RNA was determined by RT-qPCR assay; (B) GFP
609 expression was observed in Caco-2 or Caco-2-N cells using microscopy at indicated
610 time point after inoculation; Representative images from one of three independent

611 experiments. (C) Cell lysates were resolved by SDS-PAGE and probed with anti-
612 Spike and anti-Tubulin antibodies. Representative images from two independent
613 experiments; (D) The total RNAs were extracted and RT-qPCR assays were
614 conducted to determine viral RNA levels. Error bars represent the standard deviations
615 from one of two independent experiments performed in triplicate; (E) RT-PCR
616 analysis of the SARS-CoV-2 GFP/ΔN genome in Caco-2-N cells infected with
617 recombinant virus using a primer set flanking the N region. The expected DNA sized
618 were indicated in each genome, and DNA marker is shown on the left. Representative
619 images from one of two independent experiments; (F-G) Recombinant SARS-CoV-2
620 GFP/ΔN virus was incubated with indicated doses of neutralizing mAbs against
621 SARS-CoV-2 (1F11 and 2F6) or HIV (VCR01), as well as soluble human ACE2-Fc or
622 F10sFV for 1 h prior to inoculation. The infection was analyzed by GFP expression 2
623 days later, and the number of positive cells was expressed as a percentage of that for
624 the VRC01 or F10sFV treatment control. Error bars represent the standard deviations
625 from three independent experiments (n=6). ***, $P < 0.001$. Significance assessed by
626 one-way ANOVA.
627
628

629

Figure 3

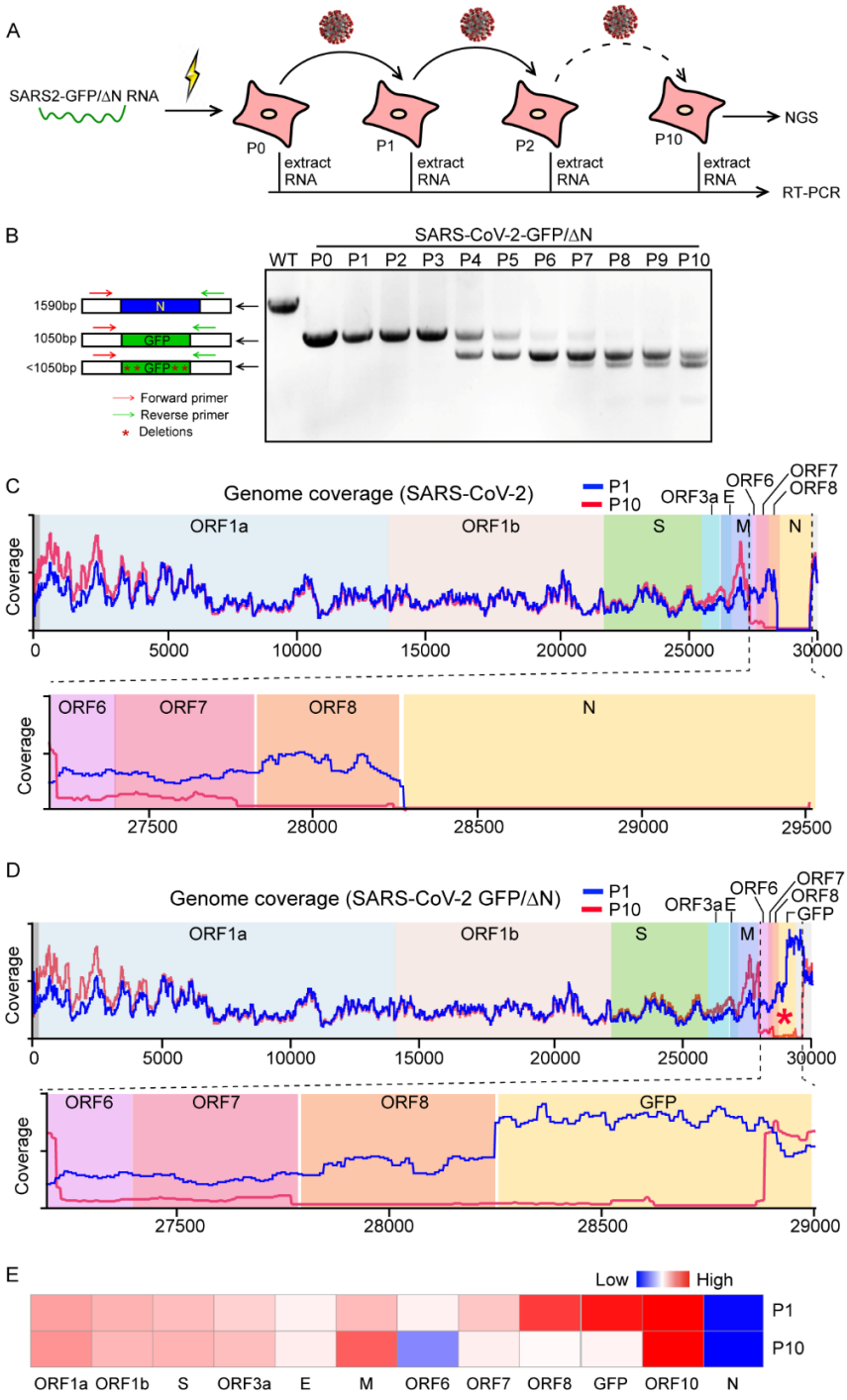


630 **Figure 3. Characterization of the genetic stability of SARS-CoV-2 GFP/ΔN trVLP.**

631 (A) Detection of the GFP reporter gene during viral passage. RNAs were extracted from

632 the VLP infected cells of P0 to P10 passage, respectively. (B) RT-PCR was performed

633 with a primer pair flanking the N region of ORF8 and 3'UTR. The PCR products were
634 resolved on an agarose gel using electrophoresis. The numbers of time points-samples-
635 passage were denoted on the top of each lane. Representative images from one of three
636 independent experiments; (C-D) RNA-seq coverage of viruse derived reads aligned to
637 SARS-CoV-2 (C) or SARS-CoV-2 GFP/ΔN (D) genome, respectively. (E) Heatmap
638 shows the expression levels of each subgenomic RNA of P1 or P10 trVLP.
639
640

641

Figure 4

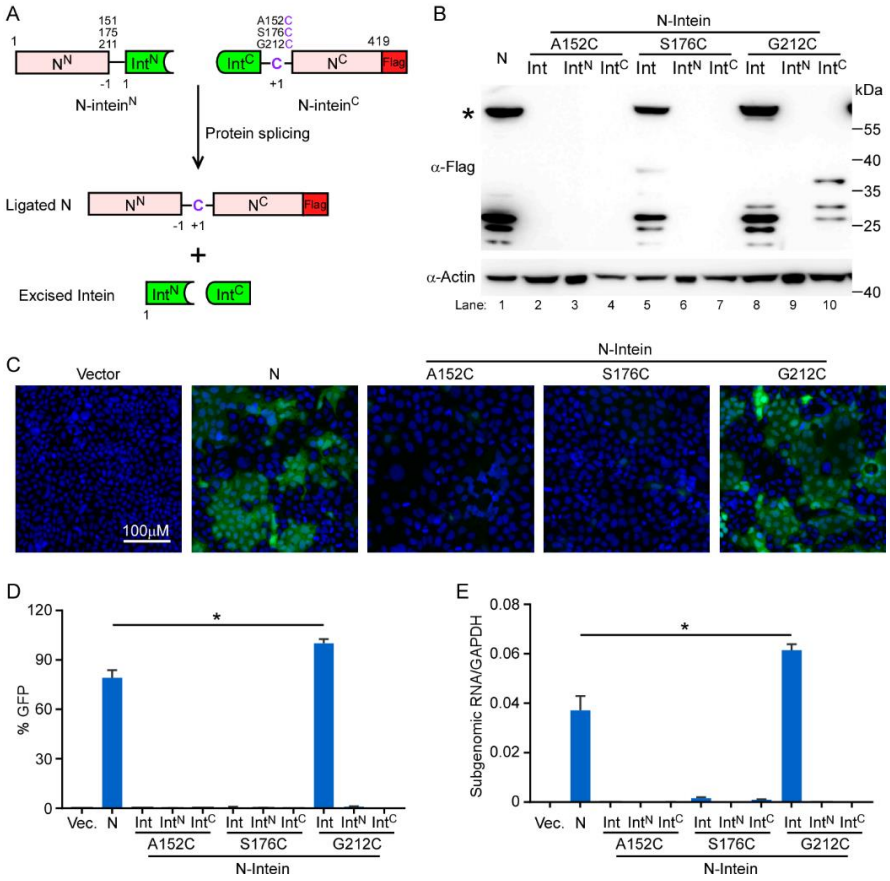


642 **Figure 4. Reconstitution of functional N protein by intein-mediated protein**
643 **splicing.** (A) Scheme depicting of intein-mediated protein trans-splicing to reconstitute
644 full length N protein. (B) Western blot (WB) analysis of lysates from Caco-2 cells
645 transduced with either full-length N or intein-N lentiviruses. The star indicates the full-
646 length N protein. The WB is representative of three independent experiments. (C) GFP
647 fluorescence in Caco-2-N cells infected cell culture medium (containing SARS-CoV-2
648 GFP/ΔN progeny) collected from each Caco-2-$N^{int}$ cells which was inoculated with
649 SARS-CoV-2 GFP/ΔN trVLP at 2 days of culture. The image is representative of n=4.
650 (D) Cells were harvested to quantify GFP expression by flow cytometry analysis, and
651 (E) Subgenomic RNA of E were determined by RT-qPCR assay. Error bars represent
652 the standard deviations from one of three independent experiments performed in
653 triplicate. *, $P < 0.05$. Significance assessed by one-way ANOVA.
654

Figure 5

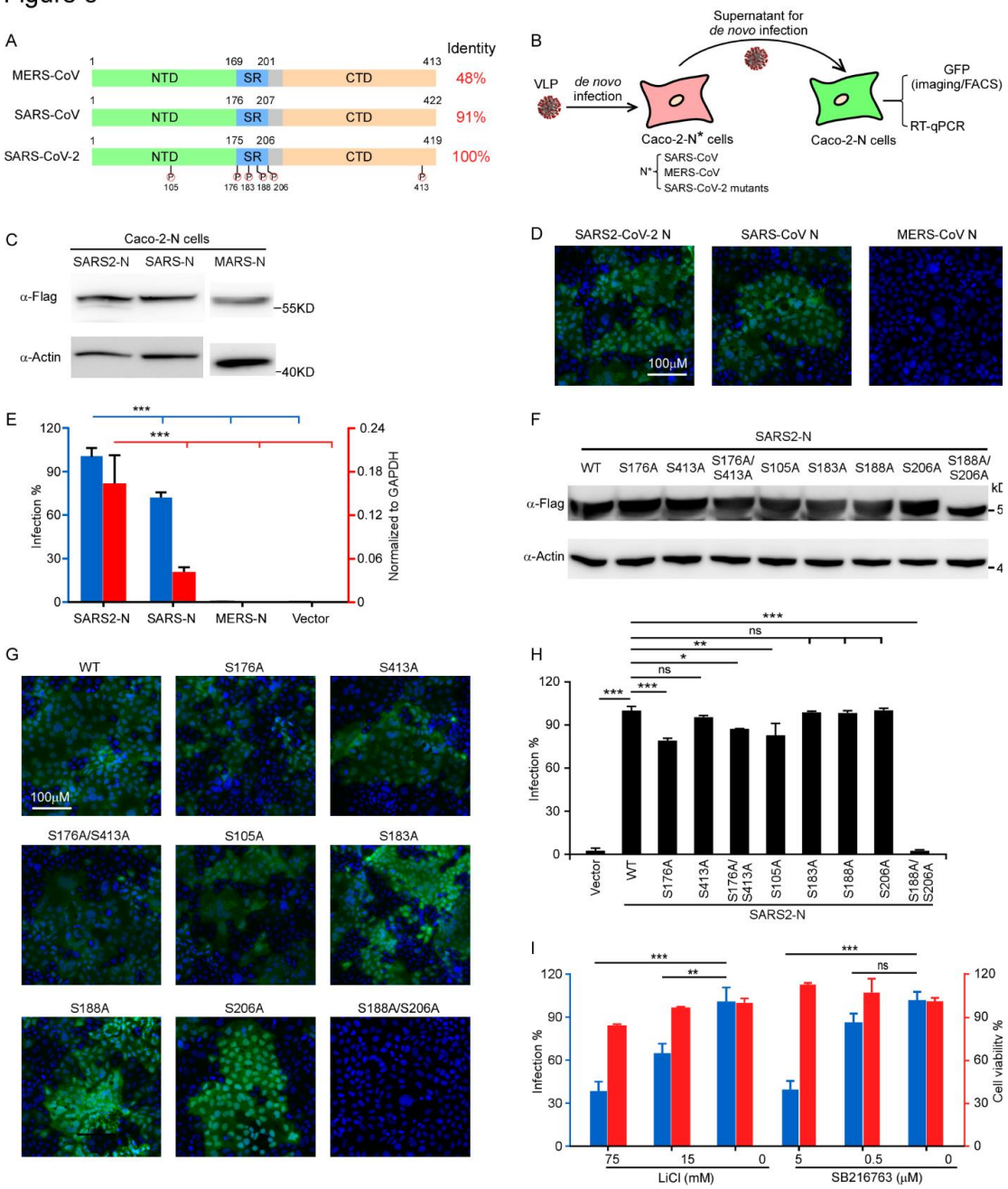


**Figure 5. Site-specific phosphorylation of N is required to support virus life cycle.** (A) Schematics and alignments of N proteins from MERS-CoV, SARS-CoV and SARS-CoV-2. The phosphorylation sites in SARS-CoV-2 N protein were highlighted. (B) Schematic presentation of assessment of N variants function. The trVLP inoculated with Caco-2 cells transduced with N variants, and the cell culture medium were

collected to infect the Caco-2-N cells, and GFP expression analyzed by flow cytometry/microscopy or viral subgenomic RNA abundance were determined by RT-qPCR. (C) Western blotting assay was performed to detect the N proteins expression in Caco-2 cells transduced with distinct N genes from SARS-CoV-2, SARS-CoV or MERS-CoV. (D-E) The cell culture medium was collected from SARS-CoV-2 GFP/ΔN trVLP infected Caco-2 cells expressing N from SARS-CoV-2, SARS-CoV or MERS-CoV to infect the naïve Caco-2-N cells. GFP were observed using microscopy and cellular RNA was extracted for RT-qPCR analysis to determine viral subgenomic RNA levels. (F) Western blotting assay detected the expression of SARS-CoV-2 N WT or mutants in Caco-2 cells. (G-H) The cell culture medium was collected from SARS-CoV-2 GFP/ΔN trVLP infected Caco-2 cells expressing SARS-CoV-2 N mutants to infect the naïve Caco-2-N cells. GFP were observed using microscopy and cellular RNA was extracted for RT-qPCR analysis to determine viral subgenomic RNA levels. (I) GSK-3 inhibitors LiCl or SB216763 treated Caco-2-N cells inoculated with SARS-CoV-2 GFP/ΔN trVLP, the cell culture medium was then inoculated with Caco-2-N cells. RNA was extracted for RT-qPCR analysis to determine viral subgenomic RNA levels. Cell viability was evaluated by CellTiter-Glo assay. Error bars (E, H and I) represent the standard deviations from one of three independent experiments performed in triplicate. n.s. no significance; *, $P < 0.05$; **, $P < 0.01$; ***, $P < 0.001$. Significance assessed by one-way ANOVA.

683

Figure 6

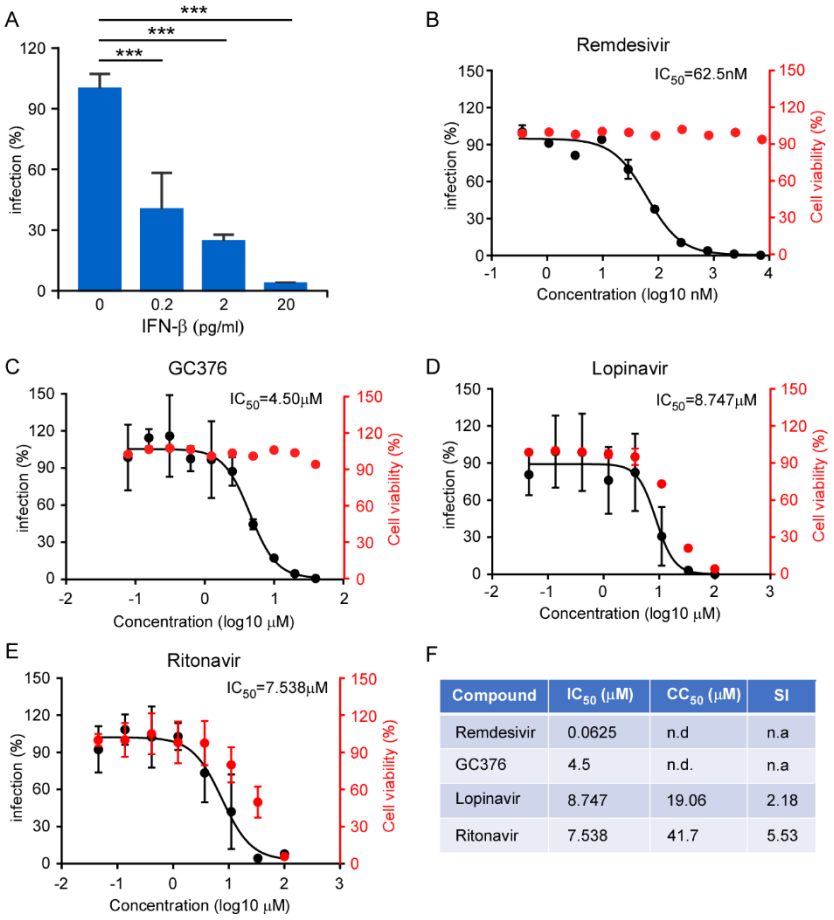


F

| Compound | $IC_{50}$ (μM) | $CC_{50}$ (μM) | SI |
|---|---|---|---|
| Remdesivir | 0.0625 | n.d | n.a |
| GC376 | 4.5 | n.d. | n.a |
| Lopinavir | 8.747 | 19.06 | 2.18 |
| Ritonavir | 7.538 | 41.7 | 5.53 |

684 **Figure 6. Inhibition of recombinant SARS-CoV-2 GFP/ΔN trVLP infection by IFN**
685 **and antivirals.** (A) IFN-β pretreated Caco-2-$N^{int}$ cells were subsequently infected with
686 trVLP and cells were subjected to flow cytometry analysis for quantify the GFP
687 fluorescence at 2 days post-infection. Error bars represent the standard deviations from
688 three independent experiments (n=6). (B-E) Antiviral effect of remdesivir, GC376,
689 lopinavir and ritonavir. The drug treated cells were infected with trVLP and GFP
690 fluorescence was quantified at 48h after infection. The cytotoxic effect of each drug at
691 indicated concentrations were determined by CellTiter-Glo cell viability assay. The
692 virus infection or cytotoxicity is plotted versus compound concentration (n=3 biological
693 replicates for all compounds). The black dots indicate replicate measurements, and the

694 black lines indicate dose-response curve fits. The red dots indicate cytotoxicity. $IC_{50}$
695 values were calculated using Prism software and is representative of one of three
696 independent experiments performed in triplicate. Three independent experiments had
697 similar results. (F) Comparison of antiviral activity and cytotoxicity of each compound.
698 Selectivity Index (SI), a ratio that compares a drug's cytotoxicity and antiviral activity
699 was also calculated. n.d.=not detected; n.a.=not applicable.
700
701

Figure 7

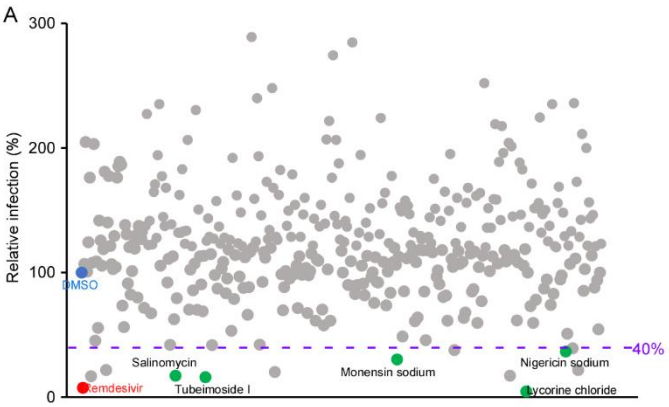


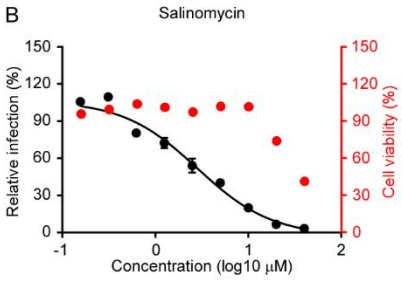


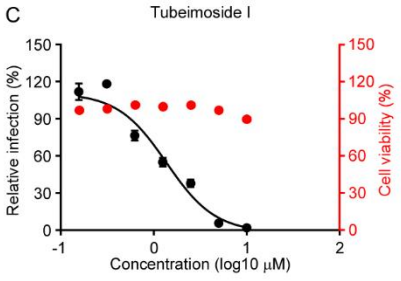


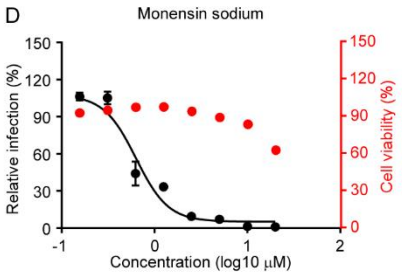


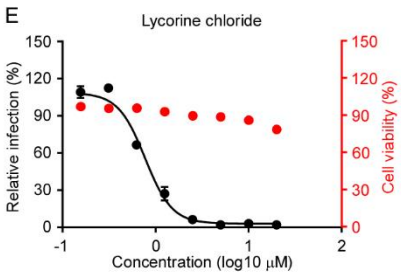


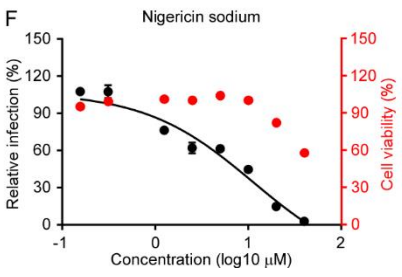


G

| Compound | $IC_{50}$ (μM) | $CC_{50}$ (μM) | SI |
|---|---|---|---|
| Salinomycin | 2.836 | 20.23 | 7.13 |
| Tubeimoside I | 1.371 | n.d. | n.a. |
| Monensin sodium | 0.632 | n.d. | n.a. |
| Lycorine chloride | 0.773 | n.d. | n.a. |
| Nigericin sodium | 11.25 | n.d. | n.a. |

**Figure 7. High throughput screening of antivirals against SARS-CoV-2 infection using trVLP system.** (A) Screening of 377 compounds from Topscience Natural Product Library and hits selection. The purple dot line represents the threshold (40%) for positive hit compounds. DMSO (blue) and remdesivir (red) are used as the control

for the screening. Each dot represents a single compound, and the green dots represent the promising candidates which exhibited potent antiviral activity without dramatic cytotoxic effect. (B-F) Dose response curves of selected hit compounds. Compounds concentrations are presented in log scale for logarithmic interpolation. Dose response curves were generated using GraphPad Prism software version 7.0. $IC_{50}$ values were calculated using Prism software and is representative of one of three independent experiments. Error bars represent the standard deviations from one of three independent experiments performed in triplicate. (G) Comparison of antiviral activity and cytotoxicity of each compound. Selectivity Index (SI), a ratio that compares a drug's cytotoxicity and antiviral activity was also calculated. n.d.=not detected; n.a.=not applicable.

# SUPPLEMENTAL FIGURES AND FIGURE LEGENDS

Fig S1

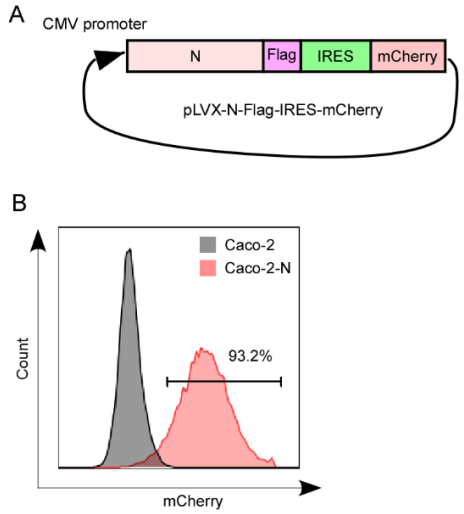


**Supplemental Figure 1. Generation of Caco-2 cell expressing SARS-CoV-2 N by lentiviral transduction.** (A) Scheme depicting the bicistronic lentiviral constructs for expressing SARS-CoV-2 N protein with C-terminal Flag tag. (B) Representative flow cytometry plots demonstrating efficient lentivirus transduction. Caco-2 cells were transduced with pLVX-N-Flag-IRES-mCherry or not transduced. Flow cytometric analysis was performed 4 d following transduction to quantify the frequencies of N-expressing cells. The flow cytometry result was representative of one of three independent experiments.

733

Fig S2

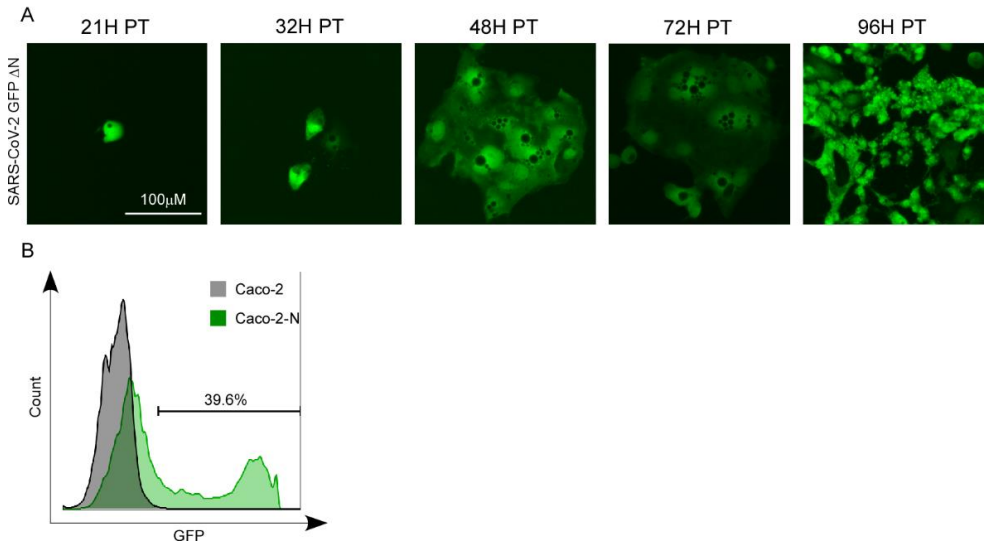


734 **Supplemental Figure 2. GFP expression in Caco-2-N cells electroporated with**
735 **SARS-CoV-2 GFP/ΔN RNA.** (A) GFP expression in Caco-2-N cells electroporated
736 with SARS-CoV-2 GFP/ΔN RNA. Caco-2-N cells were electroporated with 20 μg of
737 SARS-CoV-2 GFP/ΔN RNA. From 21h-96h p.t., GFP expression in the cells was
738 observed with microscopy. (B) GFP expression was quantified by flowcytometry at 96h
739 post transfection of the RNA. This experiment was representative of three independent
740 experiments.

741

742

743

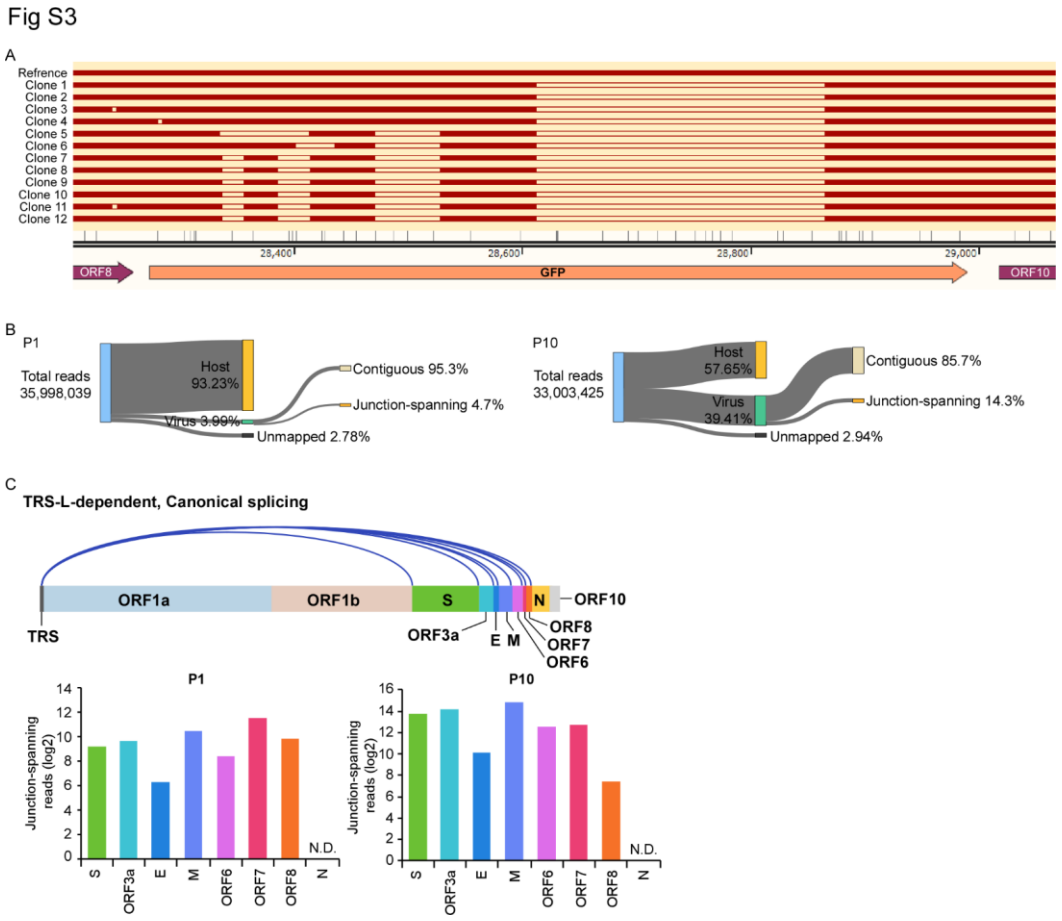


744 **Supplemental Figure 3. Characterization of the genetic stability of SARS-CoV-2**
745 **GFP/ΔN virus.** (A) RT-PCR products from P10 virus infected cell passage were cloned
746 into pEASY-Blunt vector, and 12 colonies were randomly chosen for DNA sequences
747 analysis. Multiple deletions were detected in the amplicon. (B) Categories of mapped
748 reads from P1 and P10 virus infected Caco-2-N cells. (C) Canonical discontinuous
749 transcription (top) that is mediated by TRS-L (TRS in the leader) and TRS-B (TRS in
750 the body). Quantification of junction-reads from canonical discontinuous transcripts
751 post P1 and P10 virus infection.

752

753

754

Fig S4

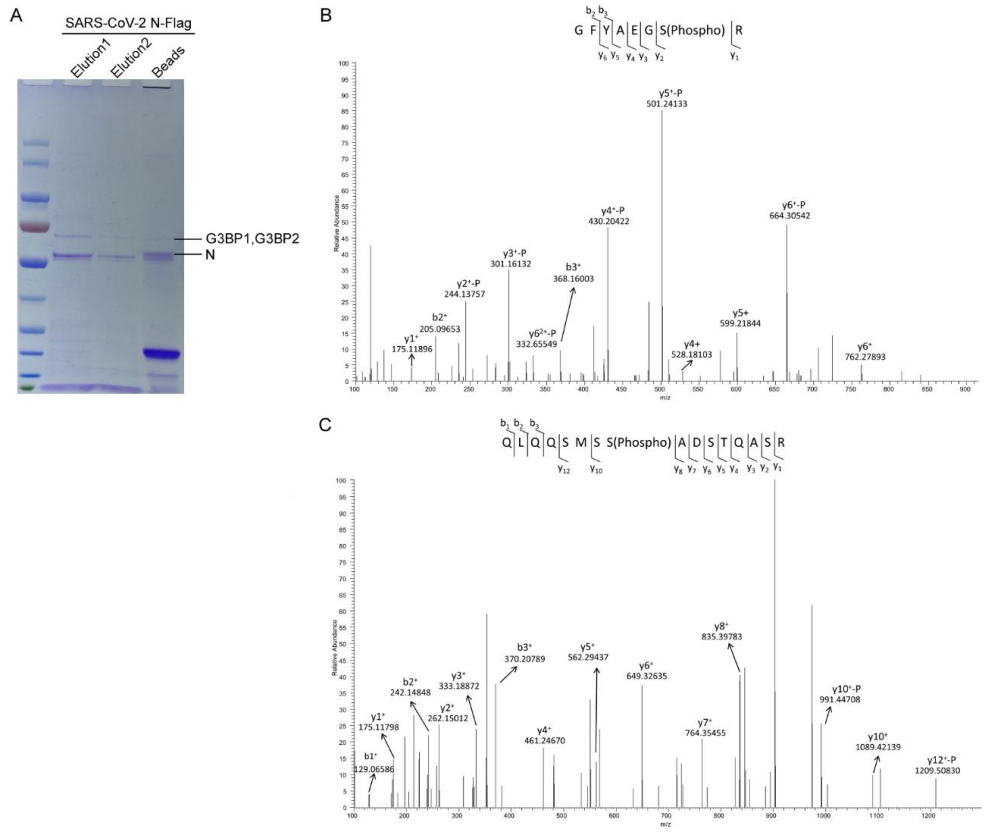


755 **Supplemental Figure 4. Identification of host factors associated with N protein and**
756 **phosphorylation on N protein by mass spectrometry.** (A) Flag tagged N protein was
757 immunoprecipitated from Caco-2-N cells infected with recombinant SARS-CoV-2
758 GFP/ΔN trVLP using Flag antibody, and the proteins were analyzed on SDS-PAGE gel.
759 The proteins were visualized by Coomassie blue staining. N, G3BP1 and G3BP2 were
760 labelled. (B) Phosphorylated peptides of N protein derived from Caco-2-N cells. Caco-
761 2-N cells in which N was C-terminal Flag-tagged were collected and cell lysates were
762 immunoprecipitated with anti-Flag coupled beads. Phosphorylated peptides of the
763 immunoprecipitates were analyzed by mass spectrometry.
764
765

# REFERENCES


1 Wang, C., Horby, P. W., Hayden, F. G. & Gao, G. F. A novel coronavirus outbreak of global health concern. *Lancet* **395**, 470-473, doi:10.1016/S0140-6736(20)30185-9 (2020).

2 Rome, B. N. & Avorn, J. Drug Evaluation during the Covid-19 Pandemic. *N Engl J Med* **382**, 2282-2284, doi:10.1056/NEJMp2009457 (2020).

3 Fung, T. S. & Liu, D. X. Human Coronavirus: Host-Pathogen Interaction. *Annu Rev Microbiol* **73**, 529-557, doi:10.1146/annurev-micro-020518-115759 (2019).

4 Enjuanes, L., Almazan, F., Sola, I. & Zuniga, S. Biochemical aspects of coronavirus replication and virus-host interaction. *Annu Rev Microbiol* **60**, 211-230, doi:10.1146/annurev.micro.60.080805.142157 (2006).

5 Lai, M. M. Coronavirus: organization, replication and expression of genome. *Annu Rev Microbiol* **44**, 303-333, doi:10.1146/annurev.mi.44.100190.001511 (1990).

6 Li, F. Structure, Function, and Evolution of Coronavirus Spike Proteins. *Annu Rev Virol* **3**, 237-261, doi:10.1146/annurev-virology-110615-042301 (2016).

7 Zuniga, S. *et al.* Coronavirus nucleocapsid protein facilitates template switching and is required for efficient transcription. *J Virol* **84**, 2169-2175, doi:10.1128/JVI.02011-09 (2010).

8 Cruz, J. L. *et al.* Coronavirus gene 7 counteracts host defenses and modulates virus virulence. *PLoS Pathog* **7**, e1002090, doi:10.1371/journal.ppat.1002090 (2011).

9 Liu, D. X., Fung, T. S., Chong, K. K., Shukla, A. & Hilgenfeld, R. Accessory proteins of SARS-CoV and other coronaviruses. *Antiviral Res* **109**, 97-109, doi:10.1016/j.antiviral.2014.06.013 (2014).

10 Almazan, F. *et al.* Coronavirus reverse genetic systems: infectious clones and replicons. *Virus Res* **189**, 262-270, doi:10.1016/j.virusres.2014.05.026 (2014).

11 Xie, X. *et al.* An Infectious cDNA Clone of SARS-CoV-2. *Cell Host Microbe* **27**, 841-848 e843, doi:10.1016/j.chom.2020.04.004 (2020).

12 Hou, Y. J. *et al.* SARS-CoV-2 Reverse Genetics Reveals a Variable Infection Gradient in the Respiratory Tract. *Cell* **182**, 429-446 e414, doi:10.1016/j.cell.2020.05.042 (2020).

13 Ju, B. *et al.* Human neutralizing antibodies elicited by SARS-CoV-2 infection. *Nature* **584**, 115-119, doi:10.1038/s41586-020-2380-z (2020).

14 Zhou, T. *et al.* Structural basis for broad and potent neutralization of HIV-1 by antibody VRC01. *Science* **329**, 811-817, doi:10.1126/science.1192819 (2010).

15 Chan, K. K. *et al.* Engineering human ACE2 to optimize binding to the spike protein of SARS coronavirus 2. *Science* **369**, 1261-1265, doi:10.1126/science.abc0870 (2020).

16 Li, Y. *et al.* Potential host range of multiple SARS-like coronaviruses and an improved ACE2-Fc variant that is potent against both SARS-CoV-2 and SARS-CoV-1. doi:10.1101/2020.04.10.032342 (2020).

17 Quéromès, G. *et al.* Characterization of SARS-CoV-2 ORF6 deletion variants detected in a nosocomial cluster during routine genomic surveillance, Lyon, France. *bioRxiv* (2020).

18 Addetia, A. *et al.* Identification of multiple large deletions in ORF7a resulting in in-frame gene fusions in clinical SARS-CoV-2 isolates. *J Clin Virol* **129**, 104523, doi:10.1016/j.jcv.2020.104523 (2020).

19 Riojas, M. A. *et al.* A Rare Deletion in SARS-CoV-2 ORF6 Dramatically Alters the Predicted

Three-Dimensional Structure of the Resultant Protein. *bioRxiv*, doi:10.1101/2020.06.09.134460 (2020).

20 Su, Y. C. F. *et al.* Discovery and Genomic Characterization of a 382-Nucleotide Deletion in ORF7b and ORF8 during the Early Evolution of SARS-CoV-2. *mBio* **11**, doi:10.1128/mBio.01610-20 (2020).

21 Muir, T. W. Semisynthesis of proteins by expressed protein ligation. *Annu Rev Biochem* **72**, 249-289, doi:10.1146/annurev.biochem.72.121801.161900 (2003).

22 Zettler, J., Schutz, V. & Mootz, H. D. The naturally split Npu DnaE intein exhibits an extraordinarily high rate in the protein trans-splicing reaction. *FEBS Lett* **583**, 909-914, doi:10.1016/j.febslet.2009.02.003 (2009).

23 Wu, C. H. *et al.* Glycogen synthase kinase-3 regulates the phosphorylation of severe acute respiratory syndrome coronavirus nucleocapsid protein and viral replication. *J Biol Chem* **284**, 5229-5239, doi:10.1074/jbc.M805747200 (2009).

24 Wu, C. H., Chen, P. J. & Yeh, S. H. Nucleocapsid phosphorylation and RNA helicase DDX1 recruitment enables coronavirus transition from discontinuous to continuous transcription. *Cell Host Microbe* **16**, 462-472, doi:10.1016/j.chom.2014.09.009 (2014).

25 Lokugamage, K. G. *et al.* Type I interferon susceptibility distinguishes SARS-CoV-2 from SARS-CoV. *J Virol*, doi:10.1128/JVI.01410-20 (2020).

26 Vanderheiden, A. *et al.* Type I and Type III Interferons Restrict SARS-CoV-2 Infection of Human Airway Epithelial Cultures. *J Virol* **94**, doi:10.1128/JVI.00985-20 (2020).

27 Park, A. & Iwasaki, A. Type I and Type III Interferons - Induction, Signaling, Evasion, and Application to Combat COVID-19. *Cell Host Microbe* **27**, 870-878, doi:10.1016/j.chom.2020.05.008 (2020).

28 Wang, M. *et al.* Remdesivir and chloroquine effectively inhibit the recently emerged novel coronavirus (2019-nCoV) in vitro. *Cell Res* **30**, 269-271, doi:10.1038/s41422-020-0282-0 (2020).

29 Pruijssers, A. J. *et al.* Remdesivir Inhibits SARS-CoV-2 in Human Lung Cells and Chimeric SARS-CoV Expressing the SARS-CoV-2 RNA Polymerase in Mice. *Cell Rep* **32**, 107940, doi:10.1016/j.celrep.2020.107940 (2020).

30 Siegel, D. *et al.* Discovery and Synthesis of a Phosphoramidate Prodrug of a Pyrrolo[2,1-f][triazin-4-amino] Adenine C-Nucleoside (GS-5734) for the Treatment of Ebola and Emerging Viruses. *J Med Chem* **60**, 1648-1661, doi:10.1021/acs.jmedchem.6b01594 (2017).

31 Sheahan, T. P. *et al.* Broad-spectrum antiviral GS-5734 inhibits both epidemic and zoonotic coronaviruses. *Sci Transl Med* **9**, doi:10.1126/scitranslmed.aal3653 (2017).

32 Warren, T. K. *et al.* Therapeutic efficacy of the small molecule GS-5734 against Ebola virus in rhesus monkeys. *Nature* **531**, 381-385, doi:10.1038/nature17180 (2016).

33 Flexner, C. HIV-protease inhibitors. *N Engl J Med* **338**, 1281-1292, doi:10.1056/NEJM199804303381808 (1998).

34 Cao, B. *et al.* A Trial of Lopinavir-Ritonavir in Adults Hospitalized with Severe Covid-19. *N Engl J Med* **382**, 1787-1799, doi:10.1056/NEJMoa2001282 (2020).

35 Shen, L. *et al.* High-Throughput Screening and Identification of Potent Broad-Spectrum Inhibitors of Coronaviruses. *J Virol* **93**, doi:10.1128/JVI.00023-19 (2019).

36 Alonso-Caplen, F. V., Matsuoka, Y., Wilcox, G. E. & Compans, R. W. Replication and

morphogenesis of avian coronavirus in Vero cells and their inhibition by monensin. *Virus Res* **1**, 153-167, doi:10.1016/0168-1702(84)90070-4 (1984).

37 Ianevski, A. *et al.* Potential Antiviral Options against SARS-CoV-2 Infection. *Viruses* **12**, doi:10.3390/v12060642 (2020).

38 Morens, D. M. & Fauci, A. S. Emerging Pandemic Diseases: How We Got to COVID-19. *Cell* **182**, 1077-1092, doi:10.1016/j.cell.2020.08.021 (2020).

39 Gordon, D. E. *et al.* A SARS-CoV-2 protein interaction map reveals targets for drug repurposing. *Nature* **583**, 459-468, doi:10.1038/s41586-020-2286-9 (2020).

40 Savastano, A., Ibáñez de Opakua, A., Rankovic, M. & Zweckstetter, M. Nucleocapsid protein of SARS-CoV-2 phase separates into RNA-rich polymerase-containing condensates. *Nature Communications* **11**, 6041, doi:10.1038/s41467-020-19843-1 (2020).

41 Cascarina, S. M. & Ross, E. D. A proposed role for the SARS-CoV-2 nucleocapsid protein in the formation and regulation of biomolecular condensates. *FASEB J* **34**, 9832-9842, doi:10.1096/fj.202001351 (2020).

42 Ju, X. *et al.* Identification of functional cis-acting RNA elements in the hepatitis E virus genome required for viral replication. *PLoS Pathog* **16**, e1008488, doi:10.1371/journal.ppat.1008488 (2020).